REPORT DOCUMENTATION PAGE

Form Approved
OMB No. 0704-0188

1. REPORT DATE *(DD-MM-YYYY)*	2. REPORT TYPE	3. DATES COVERED *(From - To)*
05-01-2015	Journal Article	March 2014 – Sept 2014

4. TITLE AND SUBTITLE
Biocompatible surface chemistry manipulation of gold nanorods preserves optical properties for bio-imaging applications

5a. CONTRACT NUMBER

5b. GRANT NUMBER

5c. PROGRAM ELEMENT NUMBER

6. AUTHOR(S)
Anthony B. Polito III . Elizabeth I. Maurer-Gardner . Saber M. Hussain

5d. PROJECT NUMBER
OAFW

5e. TASK NUMBER
P0

5f. WORK UNIT NUMBER
04/H04T

7. PERFORMING ORGANIZATION NAME(S) AND ADDRESS(ES)
A. B. Polito III _ E. I. Maurer-Gardner _ S. M. Hussain _
Molecular Bioeffects Branch, Bioeffects Division, Human Effectiveness Directorate, Air Force Research Laboratory,
711 HPW/RHDJ, 2729 R Street, Bldg 837,
Wright-Patterson AFB, OH 45433, USA
e-mail: saber.hussain@us.af.mil
A. B. Polito III
Department of Pharmacology & Toxicology, Boonshoft School of Medicine, Wright State University, Dayton,
OH 45435, USA

8. PERFORMING ORGANIZATION REPORT NUMBER

9. SPONSORING/MONITORING AGENCY NAME(S) AND ADDRESS(ES)
Air Force Materiel Command
Molecular Bioeffects Branch
Bioeffects Division
Human Effectiveness Directorate
711th Human Performance Wing
Air Force Research Laboratory
Wright-Patterson AFB OH 45433-5707

10. SPONSOR/MONITOR'S ACRONYM(S)
711 HPW/RHDJ

11. SPONSORING/MONITORING AGENCY REPORT NUMBER

12. DISTRIBUTION AVAILABILITY STATEMENT Distribution A: Approved for public release.PA Case Number: 88ABW-2014-6080. Date Cleared: 29 Dec 2014.

13. SUPPLEMENTARY NOTES

14. ABSTRACT Due to their anisotropic shape, gold nanorods (GNRs) possess a number of advantages for biosystem use including, enhanced surface area and tunable optical properties within the near-infrared (NIR) region. However, cetyl trimethylammonium bromide-related cytotoxicity, overall poor cellular uptake following surface chemistry modifications, and loss of NIR optical properties due to material intracellular aggregation in combination remain as obstacles for nanobased biomedical GNR applications. In this article, we report that tannic acid-coated 11-mercaptoundecyl trimethylammonium bromide (MTAB) GNRs (MTAB-TA) show no significant decrease in either in vitro cell viability or stress activation after exposures to A549 human alveolar epithelial cells. In addition, MTAB-TA GNRs demonstrate a substantial level of cellular uptake while displaying a unique intracellular clustering pattern. This clustering pattern significantly reduces intracellular aggregation, preserving the GNRs NIR optical roperties, vital for biomedical imaging applications. These results demonstrate how surface chemistry modifications enhance biocompatibility, allow for higher rate of internalization with low intracellular aggregation of MTAB-TA GNRs, and identify them as prime andidates for use in nanobased bio-imaging applications.

15. SUBJECT TERMS
Gold nanorods _ Coatings _ Biocompatible materials _ Optical properties _ Imaging

16. SECURITY CLASSIFICATION OF:			17. LIMITATION OF ABSTRACT	18. NUMBER OF PAGES	19a. NAME OF RESPONSIBLE PERSON
U					A. Polito
a. REPORT	b. ABSTRACT	c. THIS PAGE	SAR	18	19b. TELEPONE NUMBER (*Include area code*)
U	U	U			NA

Standard Form 298 (Rev. 8-98)
Prescribed by ANSI-Std Z39-18

J Nanopart Res (2015)17:485
DOI 10.1007/s11051-015-3162-7

RESEARCH PAPER

Surface chemistry manipulation of gold nanorods preserves optical properties for bio-imaging applications

Anthony B. Polito III · Elizabeth I. Maurer-Gardner · Saber M. Hussain

Received: 28 May 2015 / Accepted: 28 August 2015

Abstract Due to their anisotropic shape, gold nanorods (GNRs) possess a number of advantages for biosystem use including, enhanced surface area and tunable optical properties within the near-infrared (NIR) region. However, cetyl trimethylammonium bromide-related cytotoxicity, overall poor cellular uptake following surface chemistry modifications, and loss of NIR optical properties due to material intracellular aggregation in combination remain as obstacles for nanobased biomedical GNR applications. In this article, we report that tannic acid-coated 11-mercaptoundecyl trimethylammonium bromide (MTAB) GNRs (MTAB-TA) show no significant decrease in either in vitro cell viability or stress activation after exposures to A549 human alveolar epithelial cells. In addition, MTAB-TA GNRs demonstrate a substantial level of cellular uptake while displaying a unique intracellular clustering pattern. This clustering pattern significantly reduces intracellular aggregation, preserving the GNRs NIR optical properties, vital for biomedical imaging applications. These results demonstrate how surface chemistry modifications enhance biocompatibility, allow for higher rate of internalization with low intracellular aggregation of MTAB-TA GNRs, and identify them as prime candidates for use in nanobased bio-imaging applications.

Keywords Gold nanorods · Coatings · Biocompatible materials · Optical properties · Imaging

Introduction

Nanotechnology holds great potential, and nanomaterials are increasingly being developed for use in industrial, military, and consumer products including a vast array of biomedical applications (Adlakha-Hutcheon et al. 2009; Barreto et al. 2011). Recent advances in solution chemistries for synthesis of solid-phase nanomaterial technology have made it possible to manipulate gold nanomaterials into different sizes, shapes, and surface structures (Sun and Xia 2002). Among these properties, growing gold nanomaterials into rods and their surface manipulations have attracted attention due to their novel physical properties (Kelly et al. 2003). Gold nanorods (GNRs) are of

Electronic supplementary material The online version of this article (doi:10.1007/s11051-015-3162-7) contains supplementary material, which is available to authorized users.

A. B. Polito III · E. I. Maurer-Gardner · S. M. Hussain (✉)
Molecular Bioeffects Branch, Bioeffects Division, Human Effectiveness Directorate, Air Force Research Laboratory, 711 HPW/RHDJ, 2729 R Street, Bldg 837, Wright-Patterson AFB, OH 45433, USA
e-mail: saber.hussain@us.af.mil

A. B. Polito III
Department of Pharmacology & Toxicology, Boonshoft School of Medicine, Wright State University, Dayton, OH 45435, USA

Published online: 18 December 2015

particular interest due to their unique optical region absorbance, emission, and electronic properties. GNR optical properties are tunable by preparing nanofeatured structure based on their dimensional aspect ratio (AR) or through surface modification chemistry (Bouhelier et al. 2005). The AR describes the two-dimensional proportional relationship between the nanomaterial's width and height. Depending on the GNR's AR, a narrow range of light frequencies induces conduction band electron oscillation, termed surface plasmon resonance (SPR) (Liang et al. 2012). The spectral signature of the GNRs' longitudinal plasmon resonance extends into the near-infrared (NIR) region where aqueous biological tissue absorbs minimal amounts of light, which when using targeted design features will allow penetration and sensing within selected tissues. GNRs with a longitudinal SPR between 650 and 950 nm fall within the non-absorbing region of water- and carbon-based substances termed the "water window" permitting deep-tissue penetration ideal for nanobased biomedical applications (Weissleder 2001). Based on these unique characteristics, GNRs have been used in a vast array of biomedical applications, including diagnostic imaging, photo-therapies, and drug/gene delivery (Agarwal et al. 2011; Nagesha et al. 2007; Pandey et al. 2013; Pissuwan et al. 2008). Further, GNRs have also shown great potential as multifunctional nanoparticles termed by some as "theranostics" that combined diagnostic imaging and therapeutic applications (Choi et al. 2012; Jelveh and Chithrani 2011; Wang et al. 2009; Yang et al. 2013). However, the combination of responses from GNR including elicited toxicity, poor cellular uptake, and loss of NIR optical properties due to intracellular aggregation remains obstacles for nanobased biomedical applications (Alkilany and Murphy 2010; Panyala et al. 2009).

The toxicity of GNRs is known largely to be due to free and surface-associated cetyl trimethylammonium bromide (CTAB), a cationic surfactant used in the aqueous synthesis of GNRs (Alkilany et al. 2009; Takahashi et al. 2005; Wang et al. 2013; Wang et al. 2011). During synthesis, CTAB provides a growth micelle environment around the gold seedings, stabilizing them to form a rod (Jana et al. 2001; Nikoobakht and El-Sayed 2003). Two main strategies have been reported to overcome this surfactant's cytotoxicity: replacement by post-synthesis ligand exchange or noncovalent overcoating by chemical cover layering through electrostatic attraction (Vigderman et al. 2012a). Unfortunately, some commonly used surface modifications, for example, polyethylene glycol (PEG) functionalization, can significantly lower cellular uptake of the GNRs into cells, reducing their use in biomedical applications (Grabinski et al. 2011; Huff et al. 2007). Furthermore, overcoatings can break down in biological environments over time, resulting in surface leaching of the CTAB so chemical stabilization by overcoating does not guarantee that the CTAB toxicity is completely mitigated (Ejima et al. 2013). In addition, many surface modifications including polymer coatings and peptide functionalization are prone to particle aggregation when they are taken up by cells, resulting in loss of optical properties (Untener et al. 2013; Zhang et al. 2013). Finally, these overcoating and replacement procedures can require complicated multistep functionalization processes, (e.g., silica overcoating) that are difficult to scale up for biomedical applications (Gui and Cui 2012).

Previous studies have reported that TA-coated GNRs show reduced toxicity, demonstrate a distinctive form of endosomal uptake, and display a unique intracellular distribution pattern that reduces particle aggregation (Alkilany et al. 2009; Untener et al. 2013). Unfortunately, as the CTAB-TA GNR's AR increased, so did the toxicity, possibly due to the remaining CTAB. Therefore, to lower the toxicity, procedures for exhaustive removal or exchange of the CTAB from the GNRs may be essential. In order to address these challenges, GNRs coated with MTAB (11-mercaptoundecyltrimethylammonium bromide), a thiol analog of CTAB, have been synthesized, yet limited information is available in terms of their biocompatibility and characterization within biological matrices.

Vigderman et al. recently demonstrated by proton nuclear magnetic resonance spectroscopy that the complete replacement of CTAB with MTAB is possible, due to its analogous chemical structure (Vigderman et al. 2012b). For MTAB replacement, the CTAB micelle bilayer around the GNR was exchanged with a monolayer of MTAB that strongly binds to the GNR. The MTAB GNRs showed no toxicity in the human breast adenocarcinoma cell line, MCF-7, even at high concentrations. In addition, 40 % of MTAB GNR treatment was taken up by the cells, compared to less than 1 % of their pegylated analogs, exceeding the previously reported GNR uptake values. However, published TEM images showed extensive aggregation

of intracellular particles, causing a loss of their NIR optical priorities. In particular, the intracellular features exhibited close proximity side by side assembly of GNRs, which can result in blue shift of plasmon resonance emissions moving their GNRs spectra out of the target NIR "water window" needed for biomedical applications (Jain et al. 2006; Park 2006).

Therefore, the main aim of this study was to determine if combining MTAB GNRs with TA overcoating enhanced biocompatibility and cellular uptake, while preventing particle aggregation to preserve key NIR optical properties within the A549, an adenocarcinomic human alveolar basal epithelial cell line. The A549 cell line retains significant alveolar phenotype, and has been thoroughly characterized and used in numerous nano biocompatibility, bio-imaging, and therapeutic studies (Foster et al. 1998; Kuo et al. 2012; Mason and Williams 1980; Uboldi et al. 2009, 2012).

Materials and methods

Cell culture

The human lung, A549, cell line (ATCC) was maintained in RPMI 1640 cell culture media (ATCC) supplemented with 10 % heat-inactivated fetal bovine serum and 1 % penicillin–streptomycin. Cells were grown in a humidified incubator controlled at 37 °C and 5 % CO2. The same media composition was used for all GNR-exposure procedures.

Gold nano rods

CTAB, Silica, MTAB, and MTAB-TA GNRs were purchased from Nanopartz, Loveland, Co, USA. CTAB-TA, and PEG GNRs were synthesized as previously reported (Untener et al. 2013). Both thiol PEGs (molecular weight 20,000 and 5000) were obtained from Nanocs (Boston, MA), and tannic acid (molecular weight 1701.2) was obtained from Sigma Aldrich (St Louis, MO, USA).

GNR characterization

The purity and spectral signature of the GNRs were analyzed before the experiment, using UV–Vis spectrometry on a Bio TEK Synergy HT (Winooski, VT, USA) instrument. For evaluation of rod size and morphology, nanoparticles in solution were placed onto a formvar carbon-coated copper TEM grid (Electron Microscopy Sciences) and dried. They were imaged with transmission electron microscopy (TEM) using a Hitachi H-7600 at an accelerating voltage of 120 kV. To assess the surface charge of the GNRs, zeta potential measurements were taken using laser Doppler electrophoresis on a Malvern Zetasizer, Nano-ZS. Agglomerate sizes of the GNRs in media were determined through dynamic light scattering (DLS), also on a Malvern Zetasizer (Malvern Instruments, MA, USA).

Cellular viability assessment

A549 cell viability was evaluated using the CellTiter 96 Aqueous One Solution (MTS) (Promega) which monitors mitochondrial function and MultiTox-Glo Assay (LCDC) (Promega) which sequentially measures two protease activities; one is a marker of cell viability, and the other is a marker of cytotoxicity. Cells were seeded into a 96-well plate at a concentration of 2×10^3 cells per well and the following day treated with the stated GNR conditions. After 24 h, the cells viability was determined in accordance with the manufacturer's protocol.

Measurement of ROS generation

The intracellular generation of ROS after GNR exposure was evaluated using CM-H2DCFDA (Invitrogen) which is based on intracellular esterases and oxidation that yields a fluorescent product that is trapped inside the cell. Cells were seeded into a 96-well plate at a concentration of 2×10^3 cells per well and the following day treated with the stated GNR conditions. After 6 h, the intracellular ROS generation was determined in accordance with the manufacturer's protocol.

Quantification of intracellular GNRs

A total of 1×10^5 cells/well were seeded on 12-mm diameter glass slides in a 24-well plate in triplicate then dosed with 5 μg/mL GNRs for 24 h. The cell samples were then washed three times and treated with concentrated aqua regia for a minimum of 20 min to ensure full digestion of samples. The samples were

then diluted it to a final concentration of 3–1 % HCl to HNO3, respectively. The intracellular gold concentration was determined through inductively coupled plasma mass spectrometry (ICP-MS) on a Perkin-Elmer ICP-MS 300D instrument (Santa Clara, CA, USA). ICP-MS was conducted in standard mode with 20 sweeps per reading, at one reading per replicate, and three replicates per sample with a dwell time of 100 ms. A calibration curve was obtained using blank and four gold standard solutions (0 (blank), 2, 50, 100, and 300 μg/L), and the addition of an internal standard (bismuth) was done to ensure that no interferences were occurring.

CytoViva darkfield imaging

A549 cells were seeded at 1.25×10^5 cells per chamber on a 2-well chambered slide and grown for 24 h. The following day, the cells were given a dosage of 20 μg/mL GNRs for 24 h. After 24 h, the cells were fixed with 4 % paraformaldehyde and incubated with Alexa Fluor 555-phalloidin for actin staining and DAPI for nuclear staining (invitrogen). The slides were then sealed and imaged using a CytoViva 150 ultraresolution attachment on an Olympus BX41 microscope (Aetos Technologies, Inc.).

Hyperspectral imaging

A549 cells were seeded at 1.25×10^5 cells per chamber on a 2-well chambered slide and grown for 24 h and the following day was exposed to GNR (20 μg/ml). After 24 h, the cells were fixed with 4 % paraformaldehyde. The slides were then sealed and imaged using a CytoViva hyperspectral imaging system (Auburn, AL, USA). Image capture times and setting remained constant for all samples. Finally, hyperspectral analysis was performed using CytoViva's hyperspectral image analysis software.

Cellular internalization studies

A549 cells were seeded in a 6-well plate at 6×10^5 cells/well for 24 h and then exposed to the stated GNRs (5 and 20 μg/mL) for the indicated duration, washed, and fixed overnight in 2 % paraformaldehyde and 2 % glutaraldehyde. The cells were then stained with 1 % osmium tetroxide, washed, and subsequently dehydrated with ethanol dilutions ranging from 50 to 100 %. The cells were then embedded in LR White resin and cured overnight at 60 °C under a vacuum, after which the samples were sectioned using a Leica EM UC7 Ultramicrotome. Cell sections 70 nm in thickness were placed on a formvar carbon-coated copper TEM grid (Electron Microscopy Sciences) and were imaged. Transmission electron microscopy (TEM) was performed using a Hitachi H-7600 with an accelerating voltage of 120 kV. Care was taken to ensure full evaluation of each sectioned sample for the well-represented images.

Statistical analysis

All experimental results represent a minimum of three independent trials unless otherwise stated. Data are expressed as the mean ± the standard error of the mean (SEM). Statistical calculations were performed using SAS (Version 9.1) or GraphPad Prism (version 5.02, GraphPad Software Inc. La Jolla, CA, USA) to determine statistical significance at p values of <0.05 (*), <0.01 (**), or <0.001 (***).

Results and discussion

Gold nanorod characterization

GNR characterization was performed to determine their key physicochemical properties and to verify particle uniformity prior to experiments. TEM images demonstrated that GNR sets were uniform in size and morphology (Fig. 1, Fig. S1, Table 1, Table S1). UV–Vis analysis confirmed predicted SPR peaks based on calculated AR (Fig. 1, Fig. S2). To determine GNR surface charge, zeta potential analysis was performed on each particle (Table 1, Table S1). From this analysis, it was shown that MTAB GNRs were positively charged as expected due to MTABs quaternary ammonium cation. MTAB-TA GNRs displayed a negative surface charge, indicating that functionalization with TA was successful. When the GNRs were where exposed to a protein-rich environment (culture media), both MTAB and MTAB-TA GNRs displayed a negative surface charge, −15.5 and −18.1 mV, respectively. Hydrodynamic sizes of GNRs in media showed that TA-coated GNRs were on average larger than MTAB GNRs.

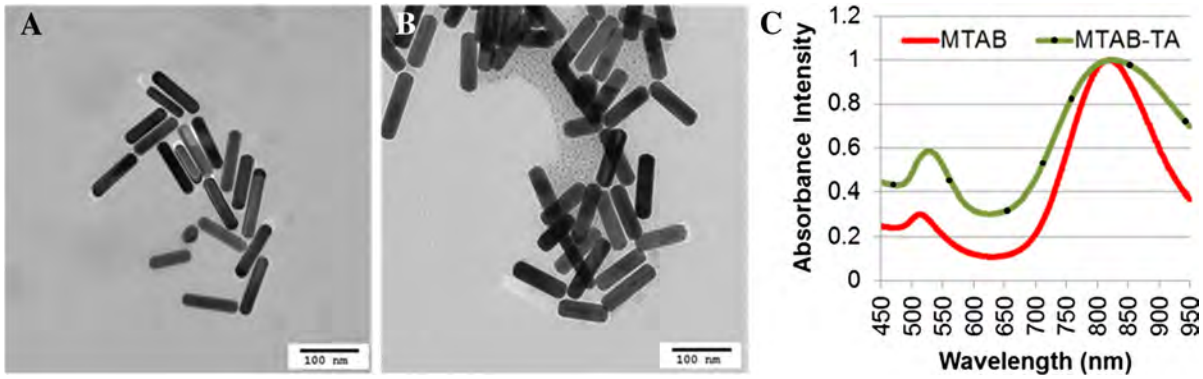

Fig. 1 Gold nanorod characterization. Representative TEM images of **a** MTAB, **b** MTAB-TA, **c** UV–Vis absorption spectra of MTAB (*red*) and MTAB-TA (*green*) GNRs. (Color figure online)

Table 1 Characterization of gold nanorods

Name	Primary size (nm)	Aspect ratio	Surface chemistry	Surface charge (mV)	Hydrodynamic diameter in media (nm)
MTAB	25 × 102 ± 4.0	4.1	MTAB	36.0	288.2 ± 4.0
MTAB-TA	25 × 104 ± 2.8	4.1	MTAB-TA	−15.7	509.6 ± 66.9

Effects of GNRs on cellular viability and stress

Since GNRs are known to exhibit toxicity linked to their physiochemical properties, we examined multiple surface chemistries, charges, ARs, and concentrations of surface modifications on toxicity by evaluating membrane integrity and mitochondrial function (Fig. S3). Overcoating CTAB and MTAB GNRs with TA resulted in enhanced biocompatibility, with no significant decrease in viability with exposure to MTAB-TA GNRs concentrations as high as 320 μg/mL (Fig. 2a). After exposure to MTAB and MTAB-TA GNRs (20 μg/ml), A549 cells showed no significant effects on their cellular viability with viability remaining over 95 % after 24 and 48 h (Fig. S4). The viability data demonstrate that the reported toxicity of CTAB-TA was not due to the TA overcoating, negative surface charge, or the AR of these GNRs, suggesting that the residual CTAB bilayer was the cause of the toxicity (Alkilany et al. 2009).

Next we examined cellular stress by measuring changes in reactive oxygen species (ROS) after cellular exposure to the various GNRs. The 6-h time point was chosen based on maximum ROS response before cell death. A549 cells showed no significant increase in ROS levels after exposure to MTAB and MTAB-TA GNRs, even at four times the treatment concentration of the CTAB GNRs that significantly increased ROS levels (Fig. 2b). Together, these results demonstrate the high biocompatibility of both MTAB and MTAB-TA GNRs. Statistical significance was determined using a one way ANOVA with Dunnett's post-hoc tests.

In view of their biocompatibility based on these initial findings and their longitudinal SPR peaks in the NIR "water window," we chose to further explore the cellular association and in vitro hyperspectral signature of MTAB AR 4 GNRs with and without a TA coating.

Cellular association and in vitro hyperspectral signature

Visualization of cellular association of MTAB and MTAB-TA GNRs was shown by darkfield microscopy (Fig. 3a–c). Both GNRs interacted with A549 cells and had a high level of cellular association. MTAB and MTAB-TA GNRs appeared to be densely packed, suggesting the associated and/or internalized GNRs are in clusters. In addition, the morphology of A549 cells were retained, further confirming the biocompatibility of the GNRs.

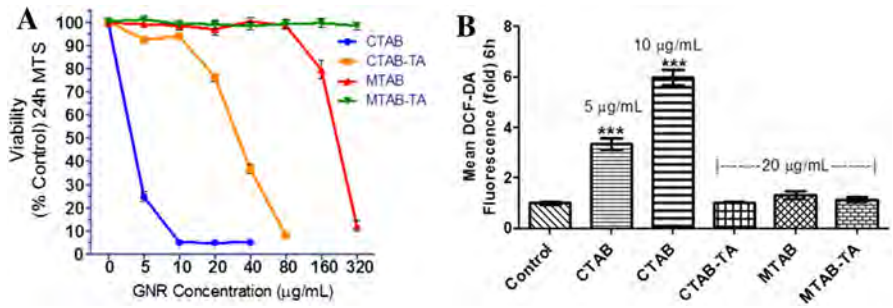

Fig. 2 Analysis of TA-coated versus uncoated GNR Biocompatibility. MTS assay results indicate the TA coating enhanced the biocompatibility of both CTAB and MTAB GNRs. **a** MTAB–TA showed no significant decrease in viability concentrations as high as 320 µg/mL. **b** ROS assay demonstrated a significant increase in ROS after exposure to CTAB GNRs at concentrations as low as 5 µg/mL

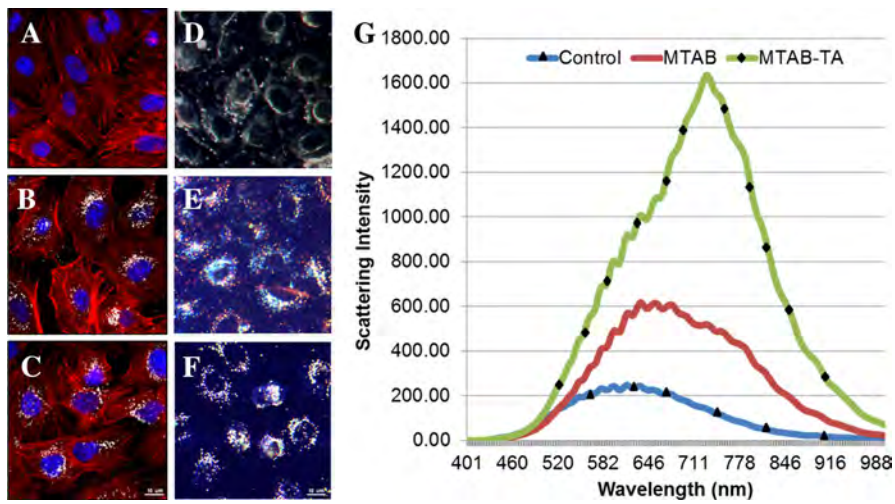

Fig. 3 Representative darkfield and hyperspectral images with analysis of intercellular GNR optical properties. Fluorescent images following GNR 20 µg/mL exposure: **a** Control, **b** MTAB, and **c** MTAB-TA. Fluorescent images results illustrate clustering of GNRs with the morphology of A549 cells retained. A549 cells underwent actin (*red*) and nuclear (*blue*) stainings with GNRs (reflecting *white*). Hyperspectral images following GNR 20 µg/mL exposure **d** Control, **e** MTAB and **f** MTAB-TA. Results revealed that MTAB-TA presented a more uniform clustering and spectral profile based on their appearance in the hyperspectral images. **g** Analysis of in vivo optical properties. MTAB hyperspectral profile (*red*) ($n = 194$) displayed low intensity and loss of NIR optical properties of GNRs. In contrast, the MTAB-TA hyperspectral profile (*green*) ($n = 385$) showed persevered NIR properties with intensity greater than 2.5 times that of the MTAB hyperspectral profile. Control (*blue*) ($n = 335$). (Color figure online)

Next we performed in vitro hyperspectral imaging (HSI) microscopy to investigate the GNR's optical properties after cellular association. HSI combines the use of darkfield microscopy and spectroscopy for the measurement of the reflectance spectrum at individual pixels in a micrograph. HSI analysis has successfully been used for characterizing gold nanoparticle aggregation, protein adsorption, and cell uptake in biological/cellular environments (Grabinski et al. 2013). This in vitro analysis of MTAB and MTAB-TA GNRs is critical, as many studies have shown that biological/cellular environments can alter the optical properties of GNRs and other nanomaterials. HSI analysis demonstrated that both GNRs had a strong association to A549 cells and appeared to indicate clustering of both MTAB and MTAB-TA GNRs (Fig. 3d, e). However, the MTAB GNRs displayed a vast array of colors compared to the primarily white appearance of

the MTAB GNRs, indicating a shift out of the NIR to the visible spectra. Further, MTAB-TA GNRs have a more uniform clustering that allows for easier identification and delineation of the GNR clusters. Next, the reflectance spectrum of individual GNR clusters were measured and compiled to create a hyperspectral profile for both MTAB and MTAB-TA GNRs (Fig. 3g). The hyperspectral analysis revealed that the spectral maxima were decreased in both hyperspectral profiles, compared to their spectral profiles as synthesized (Fig. 1). This blue shift in spectral maximas could have resulted from GNR intracellular aggregation with side-by-side assembly (Jain et al. 2006; Stacy et al. 2013). This would effectively lower the GNRs AR resulting in the changes seen in hyperspectral profile. The hyperspectral profile of MTAB-TA GNRs ($n = 385$) reveled a sharper peak still within the NIR target "water window" ($\sim$732 nm). The shift seen with the MTAB-TA GNR clusters maybe be the result of protein corona formation and/or the orientation and proximity of the GNR to each other in the clusters after cellular association (Jain et al. 2006; Mahmoudi et al. 2014). In contrast, the hyperspectral profiles of MTAB GNRs ($n = 194$) and control ($n = 335$) displayed broad peaks that were located primarily outside the target NIR window ($\sim$630–679 and $\sim$550–634 nm, respectively). In addition, MTAB-TA GNRs demonstrated a greater than 2.5-fold increase in scattering intensity after cellular association over the MTAB GNRs. Together, these results suggest that the MTAB-TA GNR form uniform GNR clusters that are able to better preserve their NIR optical properties after cellular uptake. This finding would be significant for nano-based bio-imaging and therapeutic applications as a strong spectra profile in the NIR "water window" after exposure to biological/cellular environments is required for optimum efficacy in biomedical applications.

One possible explanation of the differences in hyperspectral signature may be due to differences in GNR uptake. Another possible explanation could be due to differences in aggregation states after cellular association and/or internalization (Aaron et al. 2009). To test these possibilities, we set out to examine MTAB and MTAB-TA GNR uptake by inductively coupled plasma mass spectrometry (ICP-MS) and intracellular aggregation states by TEM.

Quantification and visualization of cellular uptake

Quantification of cellular uptake in the MTAB and MTAB-TA GNRs (5 μg/ml) was determined by ICP-MS. Both MTAB and MTAB-TA GNRs showed a high level (44 and 41 % of treatment, respectively) of cellular uptake (Fig. 4) compared to 1.5 % with PEG GNRs or 15 % with Silica-coated GNRs (Fig. S5). These results are similar to the 40 % uptake of MTAB GNRs in MCF-7 cells reported by Vigderman et al. (2012b). In addition, this finding suggests that the TA overcoating's negative surface charge has minimal impact on cellular uptake of MTAB-TA GNRs. These findings appear to differ from other studies that report that GNRs with a positive surface charge have a greater cellular association and uptake than GNRs with a negative surface charge (Hauck et al. 2008; Qiu et al. 2010). It was originally proposed that the positive surface charge on the GNRs was attracted to the negatively charged membrane of the cell resulting in higher GNR cellular association (Hauck et al. 2008). However, when GNRs of differing charge are placed in a biological environment (or simulated biological environment such as culture media), the GNRs will take in the charge of the biological environment (Qiu et al. 2010). This is in agreement with our finding that both MTAB and MTAB-TA GNRs displayed negative surface charges of 15.5 and −18.1 mV, respectively. It has been more recently proposed that the greater uptake levels seen with GNRs with a positive surface charge is because of their greater affinity to protein and the formation of a protein corona that strongly influences the GNRs cellular uptake (Nel et al. 2009; Qiu et al. 2010; Walkey and Chan 2012; Walkey et al. 2014). That TA has a strong attraction for protein and cellular membranes has been well documented (Van Buren and Robinson 1969; Wagner 1976). In addition, it has been reported that TA-coated gold NMs have strong cellular association and unique form of cellular uptake (Mukhopadhyay et al. 2012; Untener et al. 2013). To test this hypothesis, we performed SDS-PAGE to evaluate the protein corona's of the GNRs in vitro conditions (10 % FBS) and simulated in vivo conditions (100 % FBS). We found that MTAB-TA GNRs had a high level of protein association with a similar protein profile compared to MTAB GNRs (Figure S6). We further quantified the relative amounts of albumin (bands at $\sim$66 kDa) present in the MTAB-TA GNR protein corona compared with

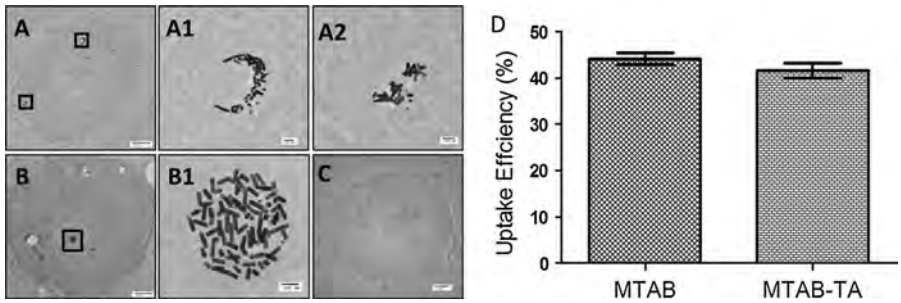

Fig. 4 Representative TEM Images and GNR Uptake by ICP-MS after exposure to 5 μg/ml for 24 h. **a** MTAB, **b** MTAB-TA, **c** control. Results demonstrate intracellular aggregation of MTAB GNRs and low aggregation of MTAB-TA GNRs. **d** Cellular uptake by ICP-MS. Results show high levels of uptakes of 44 % for MTAB and 41 % for MTAB-TA GNRs

the MTAB GNR protein corona. Results indicated that the MTAB-TA GNR had a greater relative amount of albumin association under in vitro conditions (10 % plasmon-resonance effect of FBS); however, under simulated in vivo conditions (100 % FBS), MTAB GNRs had a greater relative amount of albumin association (Figure S6). Therefore, the MTAB-TA GNRs may form a distinctive protein corona that may account for their uptake properties; thus, further research focusing on the impacts of the protein corona of TA GNRs and other NMs is needed. The finding that there is no significant difference in uptakes of the two GNRs further suggests that the difference seen between hyperspectral profiles is not significantly impacted by differences in cellular uptake of the two GNRs. Therefore, we next investigated the intracellular state of the GNRs, as previous studies have shown that the aggregation state of GNRs can affect their spectral profiles.

The distribution of MTAB and MTAB-TA GNRs AR4 (5 μg/ml) within the cell was observed using TEM (Fig. 4). MTAB-TA GNRs demonstrated low aggregation of GNRs with a unique distribution pattern/cluster within the A549 cells. In contrast, MTAB GNRs appeared aggregated in dense clusters and/or tightly packed crest shape groupings.

Visualization and analysis of intercellular distribution pattern

Since concentration can influence nanoparticle aggregation, we studied this cellular patterning at 20 μg/ml. At this new concentration, MTAB GNRs displayed small and large tightly packed clusters (Fig. 5a1, a4), crest (Fig. 5a3, 5, 6)- and doughnut (Fig. 5a2)-shaped groupings with aggregation of GNRs. MTAB-TA GNRs again displayed distinctive GNR cluster patterns with low aggregation of GNRs (Fig. 5b). Most GNRs are taken up through receptor-mediated endocytosis and further trafficked via an endo-lysosomal path (Chithrani et al. 2009). The MTAB GNRs appear to progress in the cells as follows: (1) First, small groupings of MTAB GNRs bind to the cell membrane. (2) Then the membrane invaginates with the attached MTAB GNRs and combines with similar groupings. (3) Next, GNRs can be seen as crest-shaped groupings. (4) GNRS are seen to be progressing to doughnut-shaped groupings; (5) Finally, they form as tightly packed clusters/groupings. In contrast, MTAB-TA GNRs do not display this pattern, possibly due to differences in their surface charge, protein corona, and/or a distinctive form of uptake (Hauck et al. 2008; Nel et al. 2009; Untener et al. 2013). Further, it appears that the MTAB-TA GNR clusters are less compressed/densely packed than the MTAB GNR groupings.

Next, we analyzed the GNRs clusters/groupings using ImageJ software (Schneider et al. 2012) (Fig. 6). The MTAB GNR groupings ($n = 28$) were more densely packed than the MTAB-TA GNR groupings ($n = 24$) as reflected in the area fraction of GNRs over total area of clusters/groupings values of 64 versus 50 %, respectively ($p < 0.001$). In addition, the MTAB GNR groupings had a smaller average diameter (calculated as the mean of the smallest and the largest diameter measurements for each grouping) than the average diameter of MTAB-TA GNR cluster of 343 versus 534 nm, respectively ($p < 0.001$). The total area of the MTAB-TA GNR clusters, as measured by ImageJ, appears to trend larger; however,

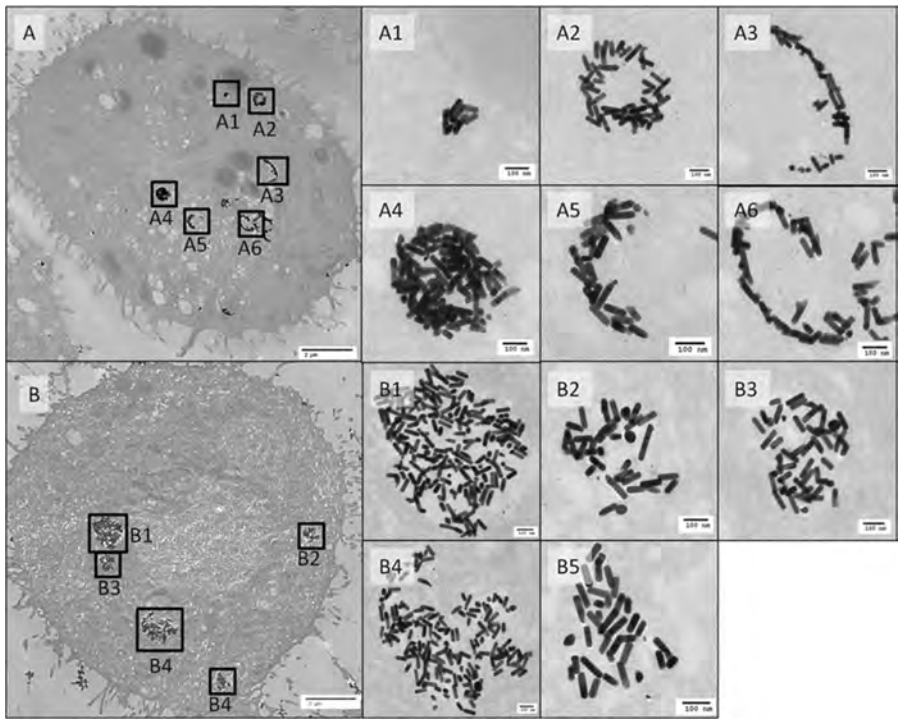

Fig. 5 Visualization of intracellular distribution pattern of MTAB-TA GNRs by TEM analysis. Representative images of **a** MTAB and **b** MTAB-TA. Results demonstrate intracellular aggregation of MTAB GNRs and low aggregation, and unique distribution of MTAB GNRs

the difference was determined not to be statistically significant ($p = 0.099$). Taken together, these results indicate that the differences in the intracellular distribution pattern may account for the preserved NIR spectral profiles of the MTAB-TA GNR clusters. Further, we examined the average diameter of extracellular GNR clusters in the TEM image using ImageJ. Results indicated that the diameter of extracellular MTAB-TA GNR clusters was larger than MTAB GNR clusters, namely, 310 versus 165 nm, respectively (Fig. S7).

Conclusions

When designing a gold nanorod for nanobased bioimaging applications, three problems are often difficult to overcome: (1) toxicity, (2) poor cellular uptake, and (3) loss of NIR optical properties due to particle aggregation in biological environments (Fig. 7).

In this study, the GNR surface chemistry was modified by replacing CTAB with MTAB and overcoating with TA. This created a novel GNR (MTAB-TA) that formed unique clusters, and showed no decrease in cellular viability, no indication of cellular stress, and no alteration of cell morphology, confirming its enhanced biocompatibility. Further, in the A549 lung cancer cell line, MTAB-TA GNRs demonstrated a cellular uptake rate 27 times greater than the commonly used PEG GNRs and 2.5 times greater than silica-coated GNRs (Fig. S5). This high uptake rate would enable a lower effective diagnostic and therapeutic working concentration. Finally, MTAB-TA GNRs displayed unique intracellular distribution patterns that not only preserved their NIR optical properties within the water but also enhanced their spectral intensity greater than 2.5 times that of uncoated GNRs. This finding is critical for bioapplications because it allows for the use of minimally invasive lasers, higher resolution imaging and more effective therapies.

In conclusion, this study has identified the complete replacement of CTAB while maintaining GNR stability and the use of TA further stabilized the GNRs so

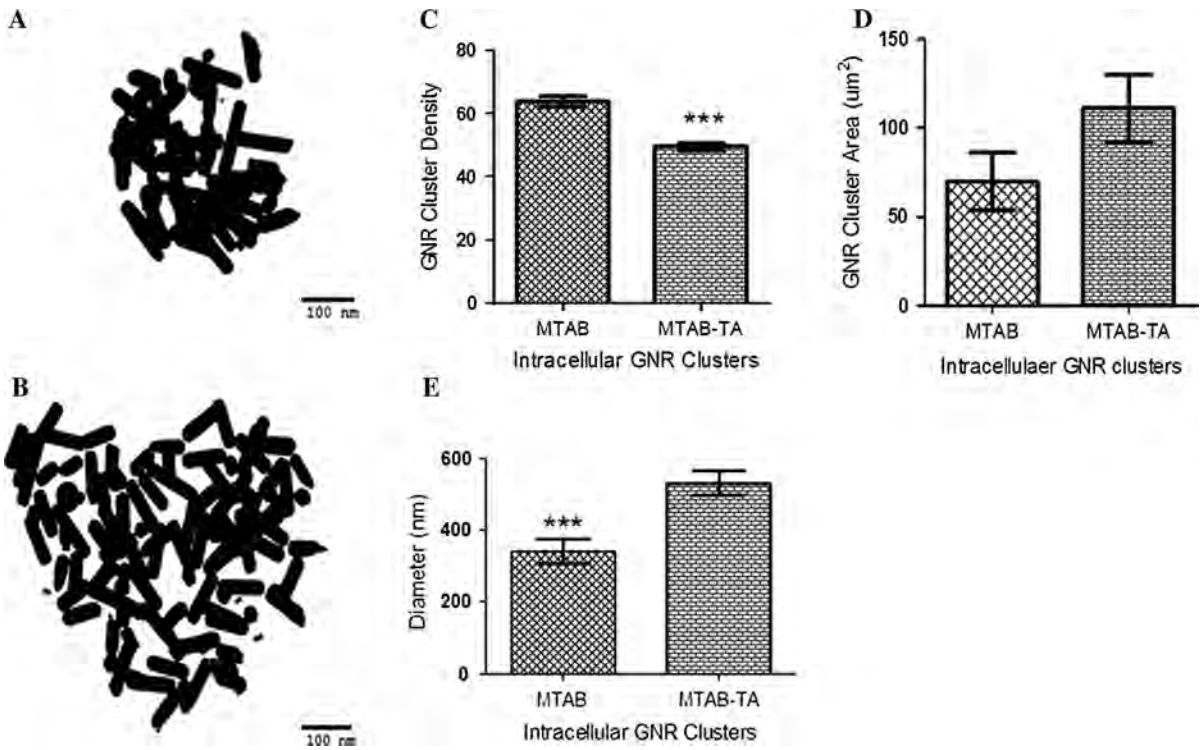

Fig. 6 Analysis of intracellular distribution pattern of GNRs by ImageJ. Representative images **a** MTAB **b** MTAB-TA **c** Average cluster density (area of GNRs/total cluster area) **d** Average cluster Area. **e** Average cluster diameter. Results demonstrate that MTAB-TA GNR Cluster ($n = 24$) are on average less densely packed and have a larger average diameter compared to MTAB GNR groupings ($n = 28$) in A549 cells. Statistical significance was determined using t-tests

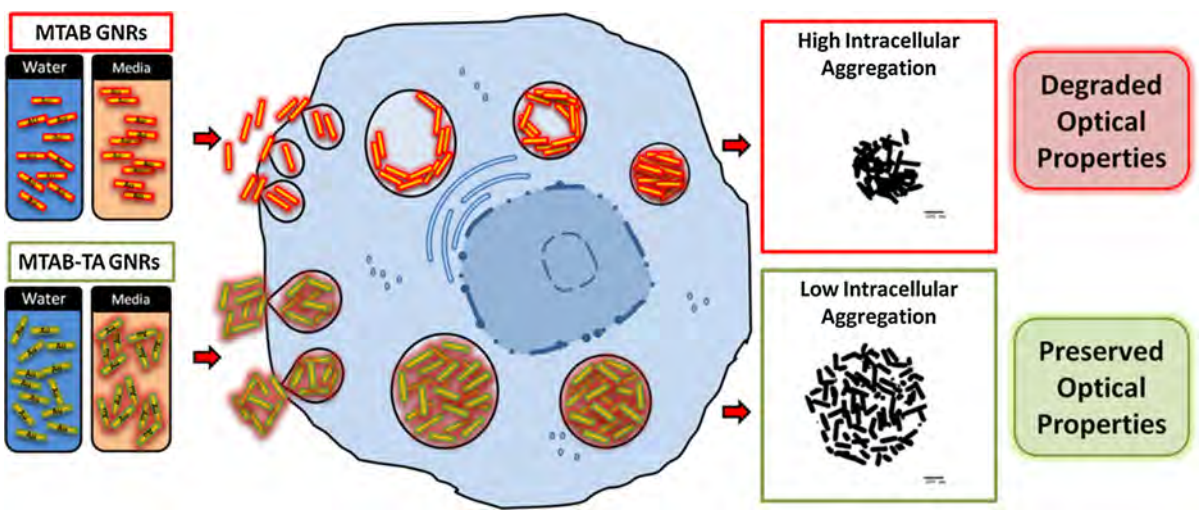

Fig. 7 Summary of the differential intracellular distribution pattern of TA-coated and uncoated MTAB GNRs. After internalization by human lung cancer cells (A549), uncoated MTAB GNRs displayed high intracellular aggregation. This resulted in a degradation of optical properties. On the contrary, TA-coated MTAB GNRs displayed low intracellular aggregation and preserved NIR optical properties

that their optical properties were preserved. Based on their biocompatible nature, high rate of in vitro cell internalization and low intracellular aggregation of MTAB-TA GNRs are prime candidates for use in vivo experimentation and nanobased bio-imaging applications.

Supporting information

Representative TEM of gold nanomaterials, UV–Vis of gold nanomaterials, characterization of gold nanomaterials, analysis of GNR biocompatibility, analysis of MTAB and MTAB-TA GNR biocompatibility, cellular uptake of GNRs, evaluation of protein corona, analysis of extracellular GNR clusters.

Acknowledgments This work was supported in part by the Air Force Surgeon General Clinical Investigations Program. Ms EI Maurer-Gardner is funded through the Henry Jackson Foundation. The authors would like to acknowledge Wright State University's Biomedical Sciences Ph.D. Program. The authors express their gratitude for the helpful suggestions of Dr LK Stolle. Distribution A. Approved for public release; distribution unlimited. (P.A. Case No. 88-ABW-2014-6080).

Compliance with ethical standards

Conflict of interest The authors declare no competing financial interest.

References

Aaron J, Travis K, Harrison N, Sokolov K (2009) Dynamic imaging of molecular assemblies in live cells based on nanoparticle plasmon resonance coupling. Nano Lett 9:3612–3618. doi:10.1021/nl9018275

Adlakha-Hutcheon G, Khaydarov R, Korenstein R, Varma R, Vaseashta A, Stamm H, Abdel-Mottaleb M (2009) Nanomaterials, nanotechnology. In: Linkov I, Steevens J (eds) Nanomaterials: risks and benefits. NATO science for peace and security series C: environmental security. Springer, Netherlands, pp 195–207. doi:10.1007/978-1-4020-9491-0_14

Agarwal A, Mackey MA, El-Sayed MA, Bellamkonda RV (2011) Remote triggered release of doxorubicin in tumors by synergistic application of thermosensitive liposomes and gold nanorods. ACS Nano 5:4919–4926. doi:10.1021/nn201010q

Alkilany AM, Murphy CJ (2010) Toxicity and cellular uptake of gold nanoparticles: what we have learned so far? J Nanopart Res 12:2313–2333. doi:10.1007/s11051-010-9911-8

Alkilany AM, Nagaria PK, Hexel CR, Shaw TJ, Murphy CJ, Wyatt MD (2009) Cellular uptake and cytotoxicity of gold nanorods: molecular origin of cytotoxicity and surface effects. Small 5:701–708. doi:10.1002/smll.200801546

Barreto JA, O'Malley W, Kubeil M, Graham B, Stephan H, Spiccia L (2011) Nanomaterials: applications in cancer imaging and therapy. Adv Mater 23:H18–H40

Bouhelier A, Bachelot R, Lerondel G, Kostcheev S, Royer P, Wiederrecht GP (2005) Surface plasmon characteristics of tunable photoluminescence in single gold nanorods. Phys Rev Lett 95:267405

Chithrani BD, Stewart J, Allen C, Jaffray DA (2009) Intracellular uptake, transport, and processing of nanostructures in cancer cells. Nanomedicine 5:118–127

Choi WI, Sahu A, Kim YH, Tae G (2012) Photothermal cancer therapy and imaging based on gold nanorods. Ann Biomed Eng 40:534–546. doi:10.1007/s10439-011-0388-0

Ejima H et al (2013) One-step assembly of coordination complexes for versatile film and particle engineering. Science (New York, NY) 341:154–157. doi:10.1126/science.1237265

Foster KA, Oster CG, Mayer MM, Avery ML, Audus KL (1998) Characterization of the A549 cell line as a type II pulmonary epithelial cell model for drug metabolism. Exp Cell Res 243:359–366. doi:10.1006/excr.1998.4172

Grabinski C, Schaeublin N, Wijaya A, D'Couto H, Baxamusa SH, Hamad-Schifferli K, Hussain SM (2011) Effect of gold nanorod surface chemistry on cellular response. ACS Nano 5:2870–2879. doi:10.1021/nn103476x

Grabinski C, Schlager J, Hussain S (2013) Hyperspectral microscopy for characterization of gold nanoparticles in biological media and cells for toxicity assessment. Methods Mol Biol 1025:167–178. doi:10.1007/978-1-62703-462-3_13

Gui C, Cui DX (2012) Functionalized gold nanorods for tumor imaging and targeted therapy. Cancer Biol Med 9:221–233. doi:10.7497/j.issn.2095-3941.2012.04.002

Hauck TS, Ghazani AA, Chan WC (2008) Assessing the effect of surface chemistry on gold nanorod uptake, toxicity, and gene expression in mammalian cells. Small 4:153–159

Huff TB, Hansen MN, Zhao Y, Cheng J-X, Wei A (2007) Controlling the cellular uptake of gold nanorods. Langmuir 23:1596–1599. doi:10.1021/la062642r

Jain PK, Eustis S, El-Sayed MA (2006) Plasmon coupling in nanorod assemblies: optical absorption, discrete dipole approximation simulation, and exciton-coupling model. J Phys Chem B 110:18243–18253. doi:10.1021/jp063879z

Jana NR, Gearheart L, Murphy CJ (2001) Wet chemical synthesis of high aspect ratio cylindrical gold nanorods. J Phys Chem B 105:4065–4067

Jelveh S, Chithrani DB (2011) Gold nanostructures as a platform for combinational therapy in future cancer therapeutics. Cancers 3:1081–1110. doi:10.3390/cancers3011081

Kelly KL, Coronado E, Coronado E, Zhao LL, Schatz GC (2003) The optical properties of metal nanoparticles: the influence of size, shape, and dielectric environment. ChemInform. doi:10.1002/chin.200316243

Kuo WS, Chang YT, Cho KC, Chiu KC, Lien CH, Yeh CS, Chen SJ (2012) Gold nanomaterials conjugated with indocyanine green for dual-modality photodynamic and

photothermal therapy. Biomaterials 33:3270–3278. doi:10.1016/j.biomaterials.2012.01.035
Liang A, Liu Q, Wen G, Jiang Z (2012) The surface-plasmon-resonance effect of nanogold/silver and its analytical applications TrAC. Trends Anal Chem 37:32–47. doi:10.1016/j.trac.2012.03.015
Mahmoudi M, Lohse SE, Murphy CJ, Fathizadeh A, Montazeri A, Suslick KS (2014) Variation of protein corona composition of gold nanoparticles following plasmonic heating. Nano Lett 14:6–12. doi:10.1021/nl403419e
Mason RJ, Williams MC (1980) Phospholipid composition and ultrastructure of A549 cells and other cultured pulmonary epithelial cells of presumed type II cell origin. Biochim Biophys Acta 617:36–50
Mukhopadhyay A, Grabinski C, Afrooz AR, Saleh NB, Hussain S (2012) Effect of gold nanosphere surface chemistry on protein adsorption and cell uptake in vitro. Appl Biochem Biotechnol 167:327–337. doi:10.1007/s12010-012-9666-z
Nagesha D, Laevsky GS, Lampton P, Banyal R, Warner C, DiMarzio C, Sridhar S (2007) In vitro imaging of embryonic stem cells using multiphoton luminescence of gold nanoparticles. Int J Nanomed 2:813–819
Nel AE et al (2009) Understanding biophysicochemical interactions at the nano–bio interface. Nat Mater 8:543–557
Nikoobakht B, El-Sayed MA (2003) Preparation and growth mechanism of gold nanorods (NRs) using seed-mediated growth method. Chem Mater 15:1957–1962
Pandey S, Shah R, Mewada A, Thakur M, Oza G, Sharon M (2013) Gold nanorods mediated controlled release of doxorubicin: nano-needles for efficient drug delivery. J Mater Sci Mater Med 24:1671–1681. doi:10.1007/s10856-013-4915-4
Panyala NR, PeñaandMéndez EM, Havel J (2009) Gold and nano-gold in medicine: overview, toxicology and perspectives. J Appl Biomed 7:75–91
Park K (2006) Synthesis, characterization, and self-assembly of size tunable gold nanorods. Dissertation, Georgia Institute of Technology, Atlanta
Pissuwan D, Valenzuela S, Cortie MB (2008) Prospects for gold nanorod particles in diagnostic and therapeutic applications. Biotechnol Genet Eng Rev 25:93–112
Qiu Y et al (2010) Surface chemistry and aspect ratio mediated cellular uptake of Au nanorods. Biomaterials. doi:10.1016/j.biomaterials.2010.06.051
Schneider CA, Rasband WS, Eliceiri KW (2012) NIH image to imageJ: 25 years of image analysis. Nat Methods 9:671–675
Stacy B, Comfort K, Comfort D, Hussain S (2013) In vitro identification of gold nanorods through hyperspectral imaging. Plasmonics 8:1235–1240. doi:10.1007/s11468-013-9538-6
Sun Y, Xia Y (2002) Shape-controlled synthesis of gold and silver nanoparticles. Science (New York, NY) 298:2176–2179. doi:10.1126/science.1077229
Takahashi H, Niidome Y, Niidome T, Kaneko K, Kawasaki H, Yamada S (2005) Modification of gold nanorods using phosphatidylcholine to reduce cytotoxicity. Langmuir 22:2–5. doi:10.1021/la0520029
Uboldi C et al (2009) Gold nanoparticles induce cytotoxicity in the alveolar type-II cell lines A549 and NCIH441. Particle and fibre toxicology 6:18. doi:10.1186/1743-8977-6-18
Untener EA, Comfort KK, Maurer EI, Grabinski CM, Comfort DA, Hussain SM (2013) Tannic acid coated gold nanorods demonstrate a distinctive form of endosomal uptake and unique distribution within cells. ACS Appl Mater Interfaces 5:8366–8373. doi:10.1021/am402848q
Van Buren JP, Robinson WB (1969) Formation of complexes between protein and tannic acid. J Agric Food Chem 17:772–777
Vigderman L, Khanal BP, Zubarev ER (2012a) Functional gold nanorods: synthesis, self-assembly, and sensing applications. Adv Mater (Deerfield Beach, Fla) 24:4811–4841, 5014. doi:10.1002/adma.201201690
Vigderman L, Manna P, Zubarev ER (2012b) Quantitative replacement of cetyl trimethylammonium bromide by cationic thiol ligands on the surface of gold nanorods and their extremely large uptake by cancer cells. Angew Chem Int Ed 51:636–641. doi:10.1002/anie.201107304
Wagner RC (1976) The effect of tannic acid on electron images of capillary endothelial cell membranes. J Ultrastruct Res 57:132–139
Walkey CD, Chan WCW (2012) Understanding and controlling the interaction of nanomaterials with proteins in a physiological environment. Chem Soc Rev 41:2780–2799. doi:10.1039/C1CS15233E
Walkey CD et al (2014) Protein corona fingerprinting predicts the cellular interaction of gold and silver nanoparticles. ACS Nano 8:2439–2455. doi:10.1021/nn406018q
Wang C, Chen J, Talavage T, Irudayaraj J (2009) Gold nanorod/Fe3O4 nanoparticle "Nano-Pearl-Necklaces" for simultaneous targeting dual-mode imaging, and photothermal ablation of cancer cells. Angewandte Chemie 121:2797–2801. doi:10.1002/ange.200805282
Wang L et al (2013) Revealing the binding structure of the protein corona on gold nanorods using synchrotron radiation-based techniques: understanding the reduced damage in cell membranes. J Am Chem Soc 135:17359–17368. doi:10.1021/ja406924v
Wang L et al (2011) Selective targeting of gold nanorods at the mitochondria of cancer cells: implications for cancer therapy. Nano Lett 11:772–780. doi:10.1021/nl103992v
Weissleder R (2001) A clearer vision for in vivo imaging. Nat Biotechnol 19:316–317
Yang HW et al (2013) Magnetic gold-nanorod/PNIPAAmMA nanoparticles for dual magnetic resonance and photoacoustic imaging and targeted photothermal therapy. Biomaterials 34:5651–5660. doi:10.1016/j.biomaterials.2013.03.085
Zhang W, Ji Y, Wu X, Xu H (2013) Trafficking of gold nanorods in breast cancer cells: uptake, lysosome maturation, and elimination. ACS Appl Mater Interfaces 5:9856–9865. doi:10.1021/am4033857
Zhang Z (2012) Mesoporous silica-coated gold nanorods as a light-mediated multifunctional theranostic platform for cancer treatment. Adv Mater (Deerfield Beach, Fla 24:1418–1423. doi:10.1002/adma.201104714

SUPPORTING INFORMATION

Supplemental method.

Evaluation of protein corona

GNRs (100 μg/mL) were exposed to either 10% FBS or 100% FBS (500 μL) and incubated at 37°C for 1 h. Samples were centrifuged at 20,000 x g for 20 min. The pellets were washed three times with 500 μL of PBS to remove the unbound proteins. The GNRs were suspended in equal parts PBS and 2x Laemmli sample buffer and were boiled for 5 min at 95°C. Finally, sodium dodecyl sulfate polyacrylamide gel electrophoresis (SDS-PAGE) was preformed to evaluate protein corona.

Supplemental figures.

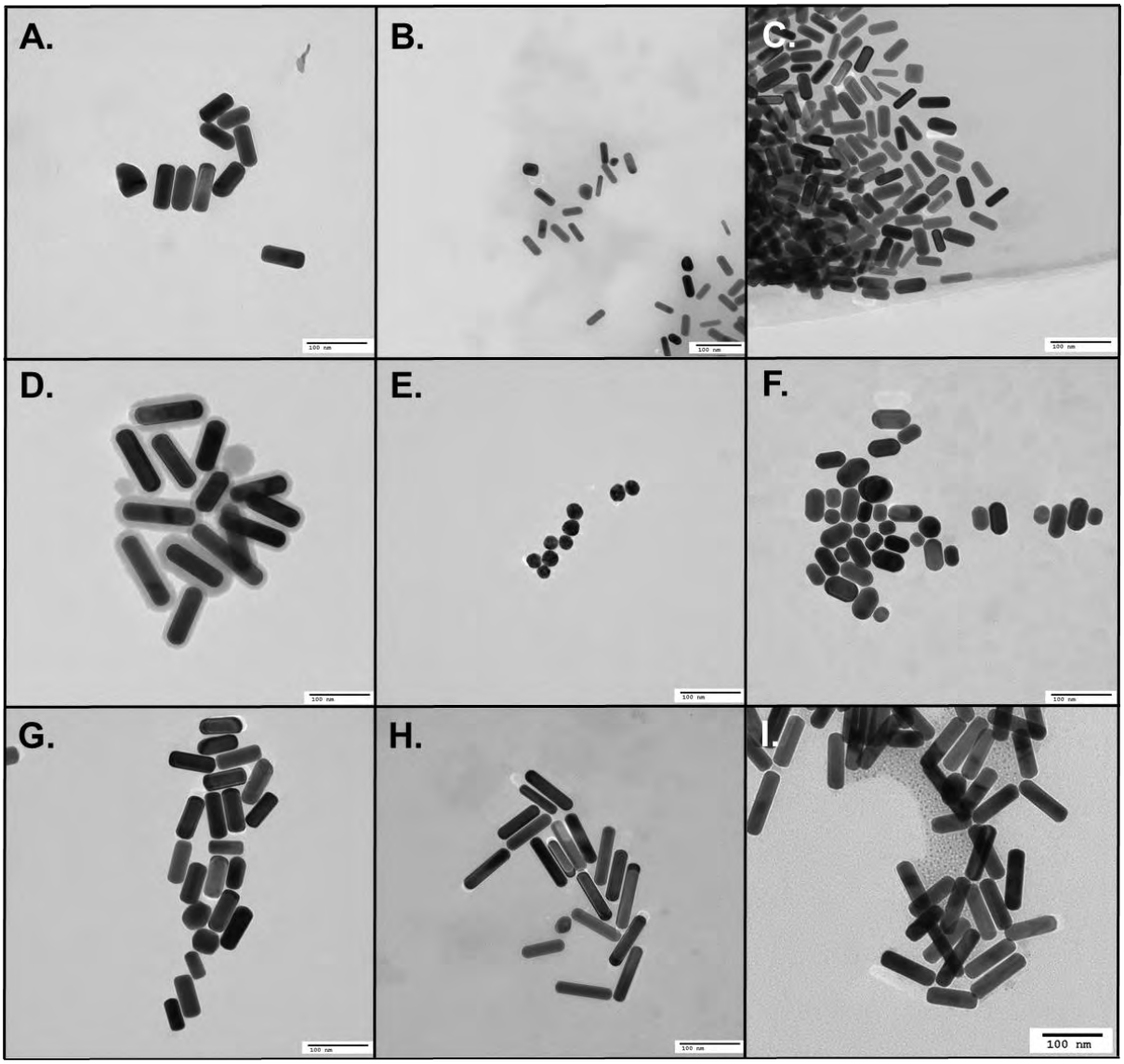

Fig. S1. Representative TEM of Gold Nanomaterials. A. CTAB, B. CTAB-TA, C. PEG, D. Silica, E. MTAB-1, F. MTAB-2, G. MTAB-3, H. MTAB-4, I. MTAB-TA

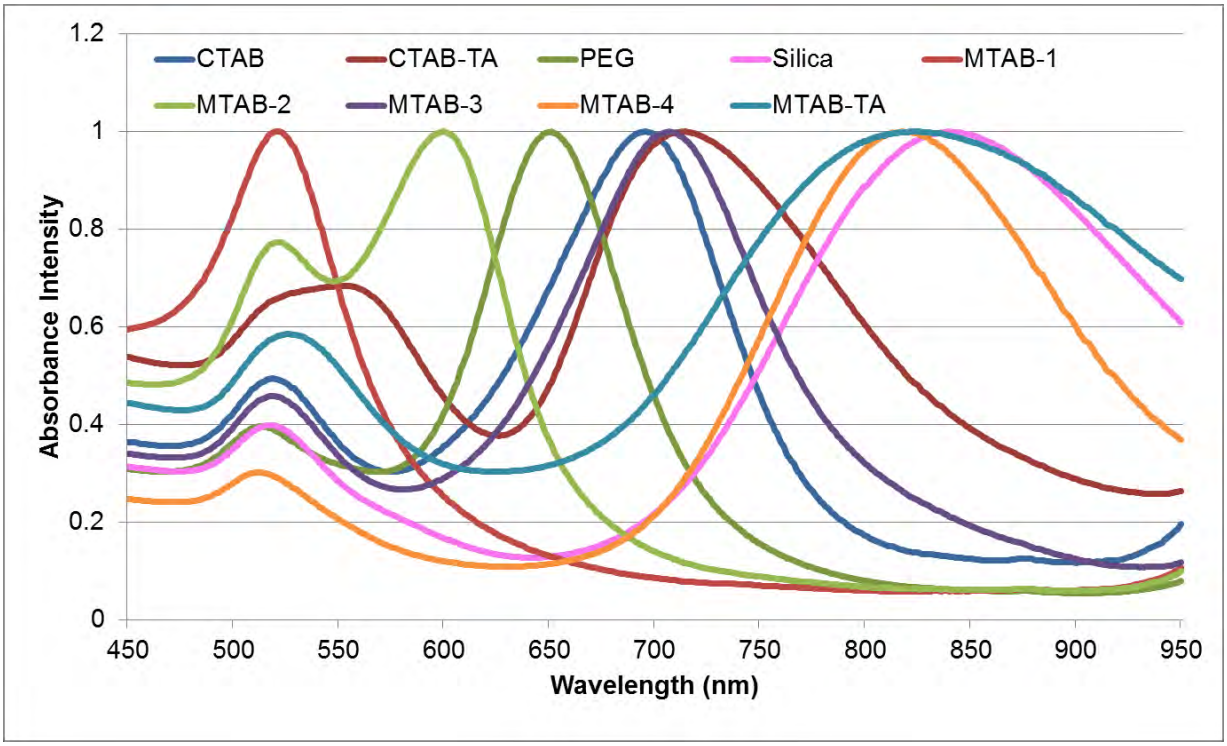

Fig. S2. UV-Vis of Gold Nanomaterials. CTAB (dark blue), CTAB-TA (dark red), PEG (dark green), Silica (pink), MTAB-1 (red), MTAB-2 (light green), MTAB-3 (purple), MTAB-4 (gold) and MTAB-TA (light blue)

Table S1. Characterization of Gold Nanomaterials

Name	Primary Size (nm)	Aspect Raito	Surface Chemistry	Surface Charge (mV)	Hydrodynamic Diameter in Media (nm)
CTAB	25x72 ±3.1	2.9	CTAB	37.2	318.7 ±4.3
CTAB-TA	22x60 ±2.1	2.8	CTAB-TA	-19.4	416.4 ±35.2
PEG	19x48 ±2.6	2.5	PEG	2.1	75.2 ±0.9
Silica	25x106 ±3.0	4.2	Mesoporous Silica	11.6	455.8 ±11.3
MTAB-1	25x25 ±1.5	1	MTAB	25.1	117.4 ±1.1
MTAB-2	25x47 ±5.4	1.9	MTAB	35.2	124.3 ±6.4

MTAB-3	25x73 ±2.7	2.9	MTAB	32.8	182.3 ±3.7
MTAB-4	25x102 ±4.0	4.1	MTAB	36.0	288.2 ±9.5
MTAB-TA	25x104 ±2.8	4.1	MTAB-TA	-15.7	509.6 ±66.9

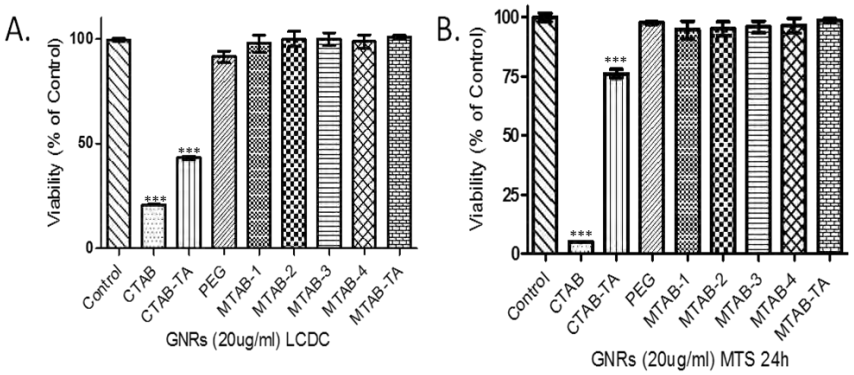

Fig. S3. Analysis of GNR Biocompatibility. A. LCDC assay and B. MTS assay results indicate GNR is biocompatibility based on surface chemistry and appears to be independent of GNR AR (1-4).

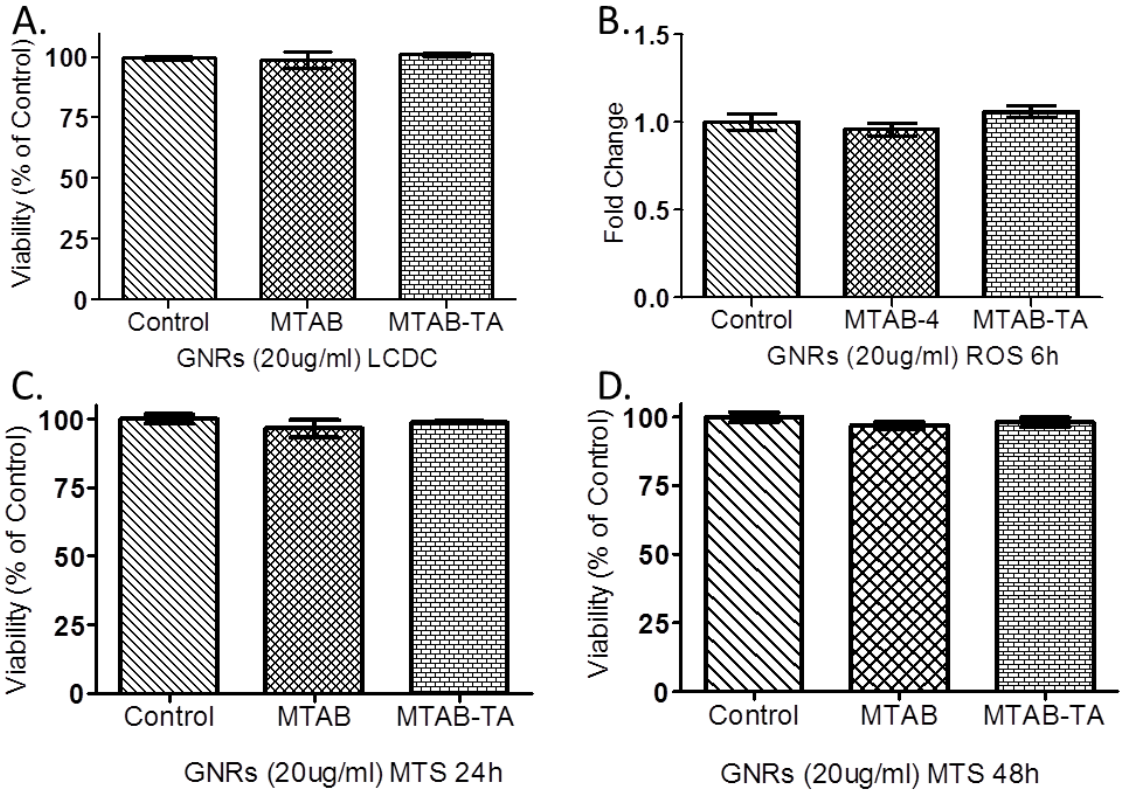

Fig. S4. Analysis of MTAB and MTAB-TA GNR Biocompatibility. A549 cells were exposure to GNR 20 μg/mL next viability, membrane integrity, ROS and mitochondrial function was determined. A. LCDC assay showed no significant decrease in viability or membrane integrity after exposure to GNRs after 24 h. B. ROS assay demonstrate no significant increase in ROS after exposure to GNRs after 6h. MTS results indicate that there is no significant change in mitochondrial function after exposure to GNRs after C. 24 h or D. 48 h. Taken together results demonstrate the high biocompatible of both MTAB and MTAB-TA GNRs.

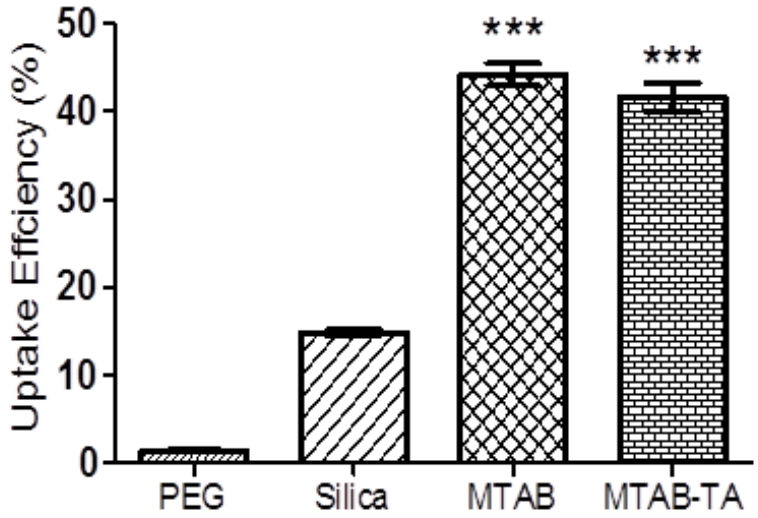

Fig. S5. Cellular Uptake of GNRs. Results show high uptake of MTAB and MTAB-TA GNRs in A549 cells compared to PEG (1.5%) or Silica (15%) coated GNRs after exposure 5 ug/ml for 24 h by ICP-MS.

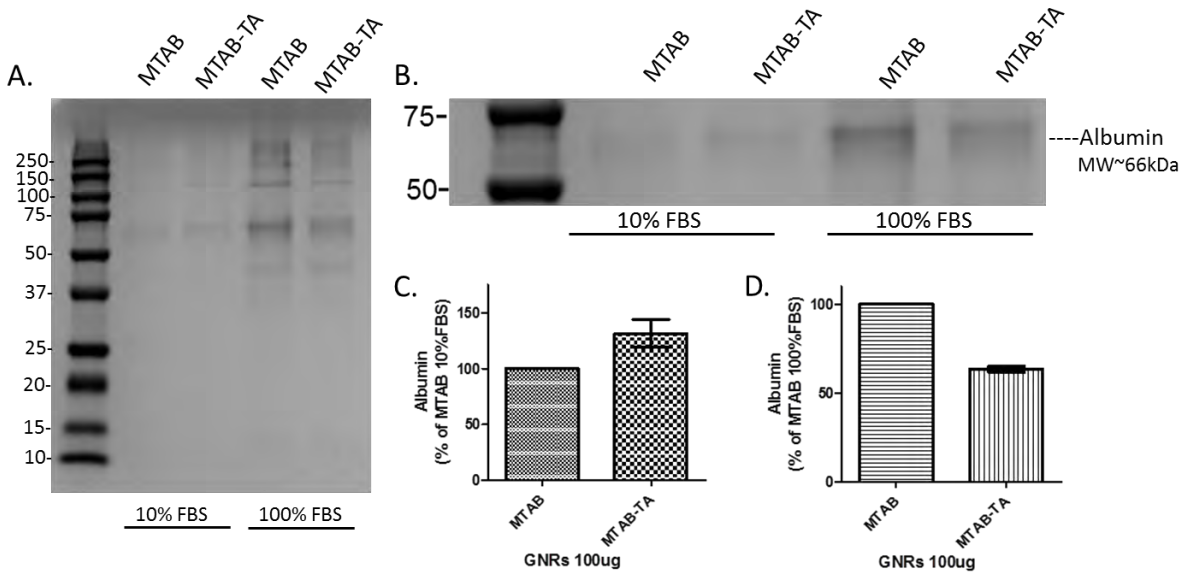

Fig S6. MTAB-TA GNRs have a high level of protein association. GNRs were exposed to 10% FBS and 100% FBS for 1 h and protein corona was evaluated by SDS-PAGE. A. MTAB-TA GNRs had a similar protein profile when compared to MTAB GNRs. B. Relative amount of albumin (bands at ~66kDa) present in GNR protein corona. C. Results indicated the MTAB-TA GNR had a greater relative amount of albumin association under in vitro conditions (10%FBS) D. However, under simulated in vivo conditions (100% FBS) MTAB GNRs had a greater relative amount of albumin association.

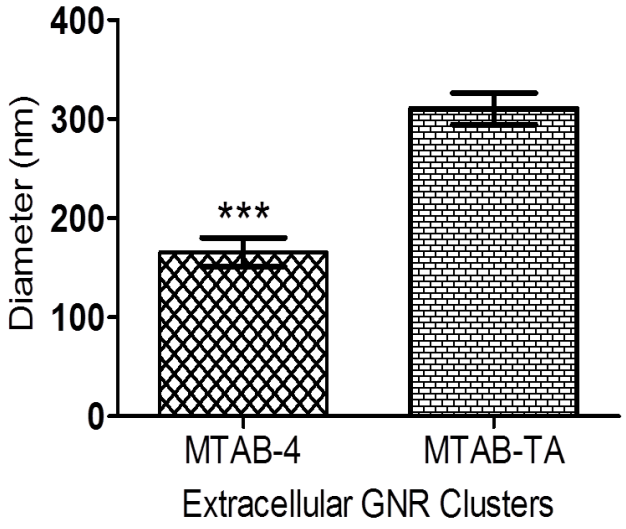

Fig. S7. Analysis of extracellular GNR Clusters. Average diameter of extracellular GNR groupings. Results suggest that MTAB-TA GNRs may form clusters prior to internalization (n=25).